Cell

Genome Analyses of Single Human Oocytes

Yu Hou,[1,6] Wei Fan,[1,4,6] Liying Yan,[1,6] Rong Li,[1] Ying Lian,[1] Jin Huang,[1] Jinsen Li,[1] Liya Xu,[1] Fuchou Tang,[1,5,*] X. Sunney Xie,[1,2,*] and Jie Qiao[1,3,*]

[1]Biodynamic Optical Imaging Center, College of Life Sciences and Center for Reproductive Medicine, Third Hospital, Peking University, Beijing 100871, China

[2]Department of Chemistry and Chemical Biology, Harvard University, Cambridge, MA 02138, USA

[3]Key Laboratory of Assisted Reproduction, Ministry of Education and Beijing Key Laboratory of Reproductive Endocrinology and Assisted Reproductive Technology, Beijing 100191, China

[4]Peking-Tsinghua Center for Life Science, Beijing 100084, China

[5]Ministry of Education Key Laboratory of Cell Proliferation and Differentiation, Beijing 100871, China

[6]These authors contributed equally to this work

*Correspondence: tangfuchou@pku.edu.cn (F.T.), xie@chemistry.harvard.edu (X.S.X.), jie.qiao@263.net (J.Q.)

http://dx.doi.org/10.1016/j.cell.2013.11.040

SUMMARY

Single-cell genome analyses of human oocytes are important for meiosis research and preimplantation genomic screening. However, the nonuniformity of single-cell whole-genome amplification hindered its use. Here, we demonstrate genome analyses of single human oocytes using multiple annealing and looping-based amplification cycle (MALBAC)-based sequencing technology. By sequencing the triads of the first and second polar bodies (PB1 and PB2) and the oocyte pronuclei from same female egg donors, we phase the genomes of these donors with detected SNPs and determine the crossover maps of their oocytes. Our data exhibit an expected crossover interference and indicate a weak chromatid interference. Further, the genome of the oocyte pronucleus, including information regarding aneuploidy and SNPs in disease-associated alleles, can be accurately deduced from the genomes of PB1 and PB2. The MALBAC-based preimplantation genomic screening in in vitro fertilization (IVF) enables accurate and cost-effective selection of normal fertilized eggs for embryo transfer.

INTRODUCTION

Successful human sexual reproduction starts with meiosis of an oocyte, which, upon fusion with a sperm cell, results in a fertilized egg whose viability is crucial to producing a healthy neonate. At the onset, every human oocyte undergoes homologous recombination of paternal and maternal genomes, which generates crossovers in individual chromosomes, contributing to genetic diversity in human evolution. Hence, each human germ cell has a unique genome, necessitating single-cell sequencing analyses, which have been recently achieved in sperm (Wang et al., 2012; Lu et al., 2012).

A normal male's sperm cell has 3%–4% probability of aneuploidy (Hunt and Hassold, 2002), chromosome abnormality due to their segregation errors, and this percentage may not change much with age (Fonseka and Griffin, 2011). Sperm cells with such aneuploidy would result in miscarriage or genetic disorders (Ferguson et al., 2007). However, aneuploidy occurs with much higher probability for the female counterpart, an oocyte, and increases drastically with the age of the female, which is one of the major causes of the decreasing live birth rate over time (Qiao et al., 2013).

Primary oocytes (four sets of chromatids, 4C) finish homologous recombination during a female's fetal period and enter a more than 10 year arrest at meiosis I. After puberty, in every menstrual cycle, one of the primary oocytes undergoes cell division, extrudes a diploid first polar body (PB1), and becomes a secondary oocyte arresting at meiosis II (Figure 1A). Upon its fertilization with a sperm cell, the secondary oocyte extrudes a haploid second polar body (PB2), and the remaining fertilized egg contains a haploid female pronucleus (FPN), as well as a haploid male pronucleus (MPN) (Figure 1B).

It is reported that crossovers in human oocytes have a frequency 1.7× higher than that of sperm (Broman et al., 1998). However, the majority of previous human oocyte crossover studies have relied on genetic linkage analyses based on family pedigree, which could be under the influence of selection. Although cytological assays of homologous recombination in the human oocytes have allowed analysis of the crossover number and distribution at the single-cell level, the resolution was relatively low (Cheng et al., 2009). Using single-cell whole-genome sequencing analyses, we have carried out the first detailed study of recombination at high resolution on human oocyte meiosis, free from the above complications.

Crossover interference along the genome has been implicated by the nonrandomly distributed crossovers (Fung et al., 2004; Jeffreys et al., 1998). Sequencing a large number of sperm cells from a person has enabled identification of individual specific recombination distribution in males (Lu et al., 2012; Wang

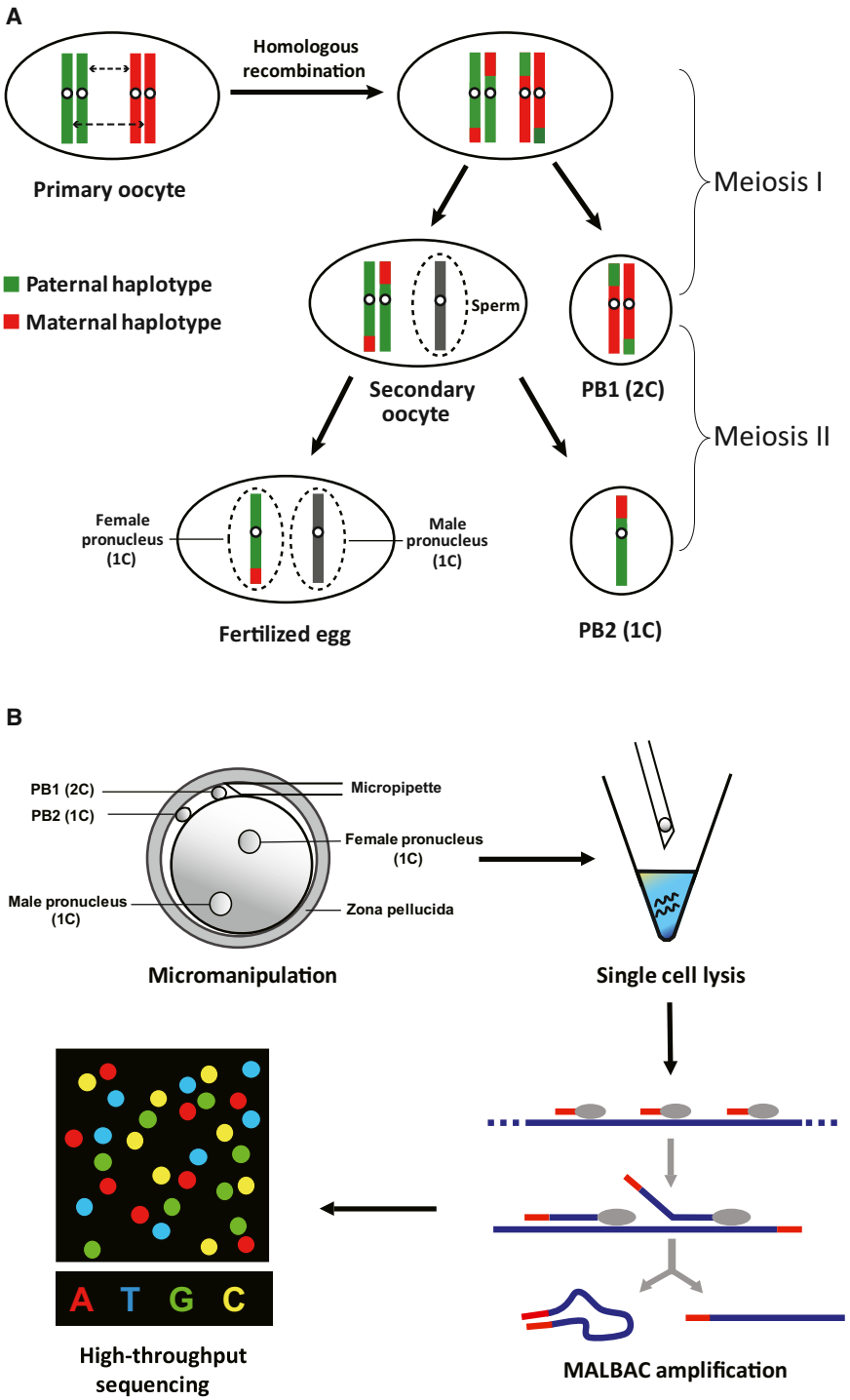

Figure 1. Schematic Charts of Human Oocyte Meiosis and Single-Oocyte MALBAC Sequencing

(A) Illustration of homologous recombination and chromosome segregation during meiosis process of human oocytes. Only one chromosome is shown with red and green colors, indicating the maternal haplotype and paternal haplotype, respectively.

(B) Flowchart of experiment procedures. The first and second polar bodies, dispensable for embryo development, were safely biopsied by a micropipette, followed by single-cell lysis, MALBAC amplification, and high-throughput sequencing. See also Figure S1.

et al., 2012), but the counterpart sequencing analysis for oocyte crossover interference has not been carried out yet. Another type of genetic interference is chromatid interference, which refers to the phenomenon that the selection of a nonsister chromatid pair for a crossover is not random but rather is affected by whether the chromatids are involved in a neighboring crossover. We have resolved these issues by simultaneously sequencing the triad of the first and second polar bodies and the female pronucleus.

This year marked the 35th anniversary of the birth of the first in vitro fertilization (IVF) baby, and IVF has resulted in more than six million test tube babies around the world. With the increased number of infertile couples, it is highly desirable to carry out single-cell sequencing analyses on individual oocytes or embryos. The PB1 and PB2, dispensable for human embryonic development, can be safely removed with a micropipette, which has been practiced for preimplantation genetic diagnosis or screening (PGD or PGS) in IVF with the goal of selecting a normal fertilized egg. To date, most of the methods for PGD/PGS, including fluorescence in situ hybridization (FISH), SNP array, and array comparative genomic hybridization (CGH) (Van den Veyver et al., 2009), cannot simultaneously detect aneuploidy and single-nucleotide variant (SNVs) associated with Mendelian diseases of severe defect phenotypes (Treff et al., 2013; Liss et al., 2011).

Here, we report the single-cell genomic studies on donated human oocytes, which were not transferred into any of the participants. Single-cell whole-genome amplification has offered high genome coverage with much reduced sequence-dependent bias. With the high coverage of MALBAC, we show that the genome of the FPN, information regarding aneuploidy, and SNVs in disease-associated alleles in particular can be accurately deduced from the genomes of PB1 and PB2 if the genetic disorders are from the mother. If the genetic disorders are from the father, one can sequence one or a few cells from the blastocyst stage

of the embryo. We demonstrate that whole-genome analyses of single human oocytes based on MALBAC allow accurate and cost-effective embryo selection for in vitro fertilization.

RESULTS

Single-Cell Whole-Genome Amplification and Sequencing of Polar Bodies and Female Pronuclei

We recruited eight healthy voluntary Asian female donors, who are 25–35 years old and have one or two healthy children from natural pregnancy, with their signed informed consent documents. The oocytes were collected using standard clinical protocols and then fertilized by intracytoplasmic sperm injection (ICSI). In total, we obtained 70 fertilized oocytes, on average 8.8 oocytes (4–15) per donor (Figure 2A).

The first and second polar bodies, as well as the female pronuclei of egg cells, were isolated with laser-assisted micromanipulation (Figure S1 available online). PB1 and PB2 were successfully biopsied from 67 (95.7%) and 64 (91.4%) oocytes, respectively. For verification purpose, the FPN of 52 (74.3%) oocytes have been biopsied. In total, 183 single cells were successfully isolated. The genome of each single cell was amplified by MALBAC and was sequenced at 0.7× depth on HiSeq 2000 (Figure 1B), obtaining genome coverage of ~32% for each single cell on average (Figure S2A and Table S1).

SNP Calling and Phasing of the Donor's Genome

We determined the heterozygous SNPs (hetSNPs) for a donor using the single-cell sequencing data of all her donated oocytes instead of sequencing the donor's blood DNA. In this study, combining sequencing data of all oocytes available from the same individual, for whom the overall sequencing depth varied from 4× to 37×, allows us to achieve individual genome coverage of 70% to 97% (Figure 2A).

Using an algorithm similar to that of population SNP calling (Bansal et al., 2010) and following a set of stringent filtering measurements, we determined 330,000–1,386,000 hetSNPs for each donor, approximately in proportion with the overall sequencing depth. Employing the donor's hetSNP information, we determined the alleles carried by each single cell at these SNP loci (Lu et al., 2012). On average, 180,000–670,000 high-confidence SNPs were determined for a single cell of each donor, which generally accounts for half of the donor's total hetSNPs.

To determine the haplotype from a donor's hetSNPs, we primarily exploited the haploid PB2 cells of the oocytes. Two independent algorithms were implemented, and the results from them were comparable, thus verifying the phasing accuracy (Figures 2B and S2B) (Kirkness et al., 2013; Lu et al., 2012). We confidently phased the haplotype on 91%–95% hetSNP loci for each donor at the whole-chromosome level. Then, crossovers on each chromosome of every individual cell were successfully inferred with the phased haplotype using a hidden Markov model (HMM) (Figures 2C, S2C, and S2D).

Female Personal Genetic Map Construction

For all donors, we identified 2,370 and 2,355 crossovers in PB2 and FPN of 55 euploid oocytes, respectively (Table S1). The average of 43 crossovers per haploid cell is ~1.65× of that in sperm. This phenomenon has been shown previously in mice that oocytes have a frequency 1.3× higher than that of sperm (Petkov et al., 2007).

These sex-specific differences likely result entirely from differences in longitudinal chromosome organization (Kleckner et al., 2003). At leptotene, chromosomes develop into a synaptonemal complex (SC), an array of chromatin loops whose bases, elaborated by proteins, comprise a longitudinal structural axis. The number of loops per micrometer of SC is relatively fixed for different sexes, regardless of the loop size. Females exhibit longer SCs than males (Tease and Hultén, 2004). Thus, female chromosomes will be organized into more loops of smaller average size (Kleckner, 2006; Novak et al., 2008). Further, recombination initiation complexes develop in association with loop bases (Panizza et al., 2011). Thus, females will have more initiation complexes and more initiating double-strand breaks (DSBs). Such proportionality of DSB number to chromosome length has been demonstrated in *C. elegans* (Mets and Meyer, 2009). DSBs develop into interhomolog interactions which, in turn, are operated upon by crossover interference. The number of crossovers is proportional to both the number of DSBs and to physical chromosome length. Proportionality of CO number and SC length has long been known for male and female in human and in other species (Kleckner et al., 2003; Tease and Hultén, 2004).

A moderate correlation (R = 0.61) was observed between the crossover numbers in the PB2 and FPN from the same oocyte (Figure 3B). Overall, crossovers do not show significant preference for FPN over PB2 in meiosis (paired Student's t test p value 0.80 and F test p value 0.79), indicating that there is no significant relationship between the haploid cell fate in meiosis II and the crossover numbers in its genome.

By binning the crossovers into 5 Mb units in the genome, we constructed the first set of female personal genetic maps, which are largely consistent with the sex-averaged map based on population analysis (HapMap) (Myers et al., 2005) and a female-specific map based on pedigree analysis (deCODE) (Kong et al., 2010) on the megabase scale (Figure 3C). Notably, chromosome X-X recombination of an individual can be analyzed by sequencing for the first time, which gave a personal chromosome X recombination rate ranging from 1.01 to 1.18 centimorgan (cM) per Mb, which is similar to the recombination pattern of autosomes (Tables S2 and S3). However, limited by the small number of oocytes for each donor, it is not feasible to detect personal recombination hot spots with statistical significance. By merging eight donors' personal genetic maps, we obtained a population genetic map that is comparable to deCODE map (Figure S3A and Table S4).

The improved amplification evenness of MALBAC allowed us to achieve high resolution in detecting crossovers with low sequencing depth (Figure 3D). About 95%, 84%, and 55% of the crossovers could be confidently assigned to intervals of 200, 100, and 30 kb, respectively. With this high resolution, we were able to study the crossover distributions at a finer genome scale. We observed a drop of recombination rates in oocyte data close to the transcription start site (TSS) (Figure 3E), reinforcing the speculation that the variation of recombination probability during oocyte meiosis, rather than selection, gives rise to the

A

Donor ID	No. of fertilized oocytes	No. of sequenced polar bodies and pronuclei	Average sequencing depth for each single cell (X)	Average genome coverage	Summed sequencing depth for each donor (X)	Summed genome coverage	No. of phased hetSNPs for each donor	No. of phased SNPs for each single cell
S01	14	35	0.9	35.6%	31.6	93.8%	1,092,055	559,567
S02	5	14	0.4	22.5%	5.4	77.4%	512,620	247,807
S03	6	15	0.4	22.1%	5.8	79.3%	512,149	241,603
S04	4	11	0.4	20.5%	3.9	69.6%	307,583	168,007
S05	12	31	0.9	34.2%	26.5	94.2%	1,046,939	527,501
S06	8	20	0.7	30.8%	14.1	90.1%	721,263	428,383
S07	6	16	0.8	32.8%	12.1	88.4%	675,195	452,225
S08	15	41	0.9	36.5%	36.7	96.6%	1,284,846	621,709
All Avg	70	183	0.7	31.7%	17.0	86.2%	769,081	405,850

B

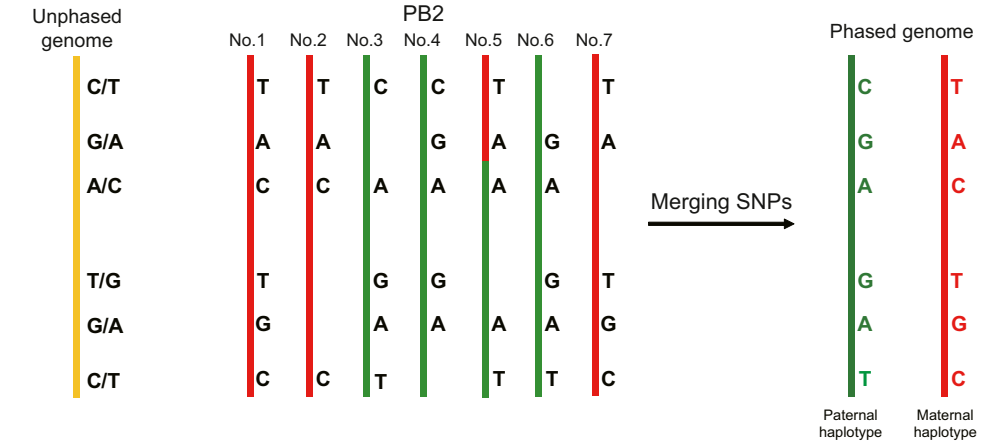

C

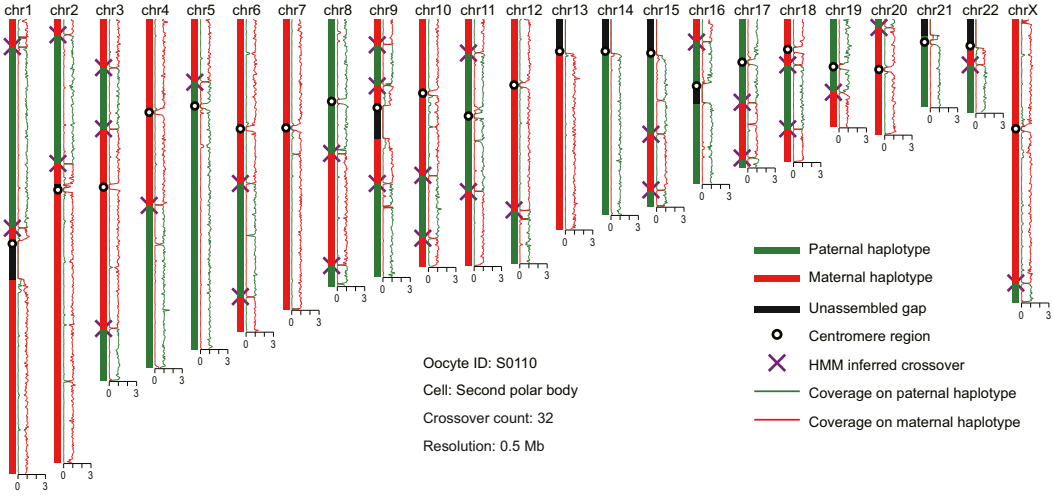

Figure 2. Calling of Heterozygous SNPs, Phasing of the Donor's Genome, and Detecting of Crossovers

(A) Summary of sequencing information for all of the single cells from eight donors. The sequencing depth and genome coverage for each cell are shown, as well as the summed values for each donor and the numbers of phased heterozygous SNPs for each donor, together with the average numbers of phased SNPs in each cell.

(B) Schematic chart of phasing the donor's heterozygous SNPs with several PB2. The genotyped SNPs for each PB2 are lined up, and the consensus SNPs are inferred for both haplotypes. Note that a rare crossover event occurs in the fifth PB2.

(C) Crossover distribution map of the 23 chromosomes from a second polar body S0110B. The normalized coverage depth that reflects chromosome copy number is shown on the right side.

See also Figure S2 and Table S1.

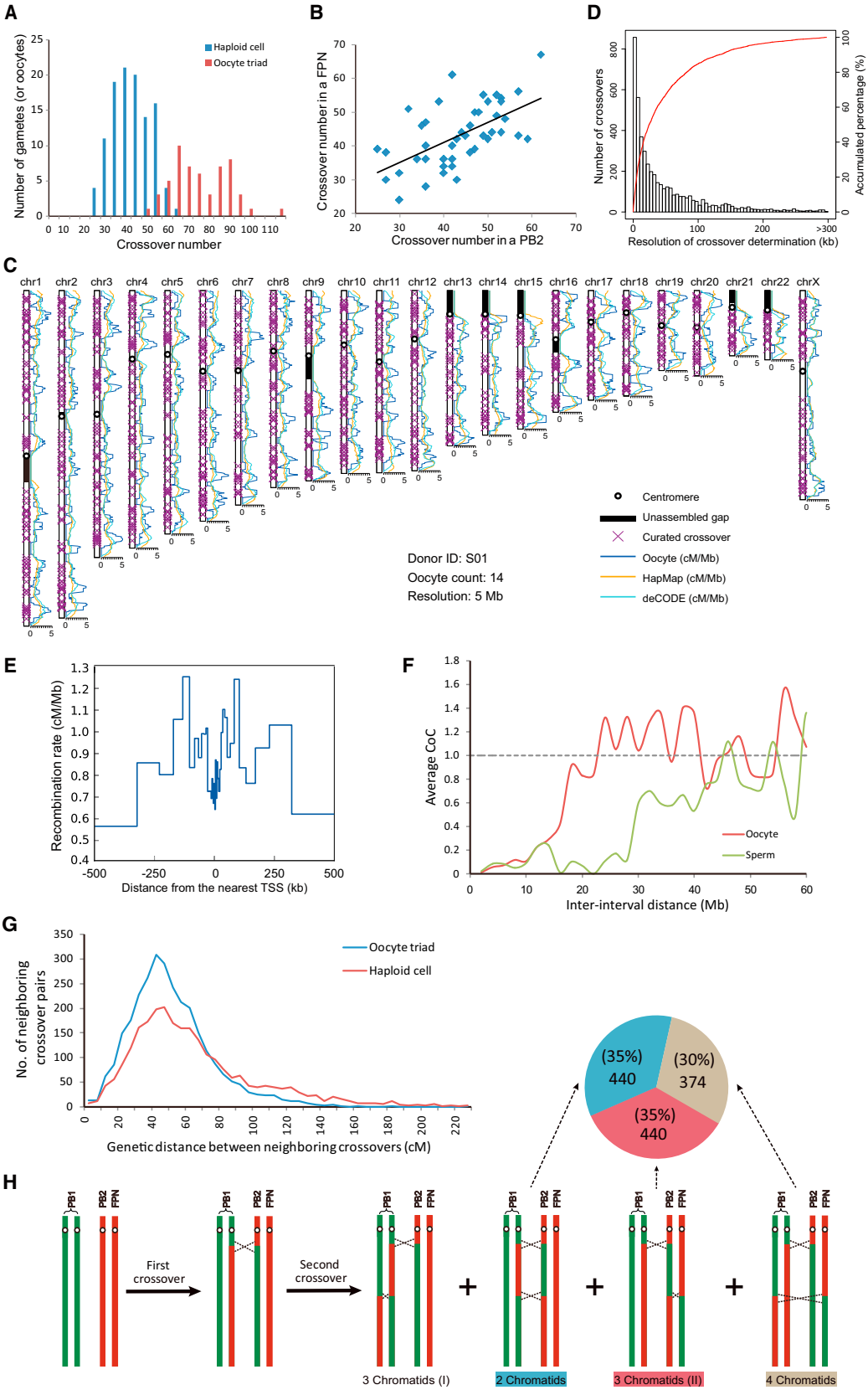

(legend on next page)

reduced recombination rate close to TSS (Coop et al., 2008). Of the crossovers unambiguously resolvable within a 10 kb interval, ~44% of these crossover intervals overlapped with at least one PRDM9 binding motif (CCnCCnTnnCCnC), which is consistent with the recently published study on single sperm cells (Lu et al., 2012) and previous population studies (Myers et al., 2008).

Crossover Interference in Human Oocytes Compared with Sperm

Crossover interference is a phenomenon that a chromosomal crossover at one position decreases the probability for another crossover occurring nearby. Crossover interference in human sperm has been recently observed by single-sperm cell sequencing (Lu et al., 2012; Wang et al., 2012). Here, we report our study of crossover interference in single human oocytes. We used coefficient of coincidence (CoC) to describe the strength of interference. This approach considers the magnitude of crossover interference as a function of the distance between crossovers along a chromosome. It provides a chromosome-wide view, irrespective of nonuniform recombination rate along the genome (Petkov et al., 2007). Figure 3F shows the CoC for the crossover interference of oocyte as a function of genetic distance (number of base pairs), as compared with that for human sperm (Lu et al., 2012). It is evident that interference acts over a smaller number of base pairs in oocytes than in sperm, which is consistent with the fact that oocytes have more crossovers per chromosome. Furthermore, the CoC curve of the neighboring crossovers on the same arms of chromosomes shows no significant difference from that of all crossovers, verifying that the crossovers across centromeres do not affect the CoC values calculated (Figure S3B).

Further analysis reveals, however, that when we plot the CoC as a function of the physical distance of the SC length (which is longer in oocytes than in sperm), the sperm and oocyte's curves overlap (Figure S3C). Analogous results have also been found in mouse (Petkov et al., 2007) and *Arabidopsis* (Drouaud et al., 2007). Crossover interference involves the spreading of an inhibitory signal along well-organized chromosomes. The fact that CoC curves for oocyte and sperm overlap when SC length is used as a metric has two mechanistic implications. First, the metric for the spreading interference signal is physical distance along the chromosome, not genomic distance in DNA/base pair length. Second, the strength of interference, i.e., the distance over which the inhibitory signal acts along the chromosomes, is exactly the same in human oocytes and spermatocytes.

Crossover interference happens between neighboring crossovers in the four sets of chromatids within the oocyte, whereas a haploid PB2 or FPN only has half of the total number of crossovers in the oocyte. We counted the crossovers of PB1, PB2, and FPN derived from the same oocyte and found that each oocyte has an average of 76 crossovers (88% of the theoretical value 43 × 2) (Table S2), and the distribution of the distance between two adjacent crossovers is shown in blue in Figure 3G. These triad data in oocytes capture more crossovers than the data from PB2 and FPN alone with only an average of 43 crossovers, providing better statistics for human oocyte crossover interference, yielding a shorter distance between two adjacent crossovers.

Weak Chromatid Interference in Human Oocytes

Another type of genetic interference, chromatid interference, refers to the phenomenon that the selection of a nonsister chromatid pair in one crossover influences the chromatid selection for a neighboring crossover (Zhao et al., 1995). Unlike the crossover interference, chromatid interference has been less studied, and the reported results are inconsistent (Chen et al., 2008; Speed et al., 1992; Teuscher et al., 2000). With the meiosis triad data here, we were able to study chromatid interference by identifying which nonsister chromatid pair is involved in each crossover. Considering the anchoring effect of centromeres, the crossover pairs were counted on the same or different chromosome arms separately.

On the same arm of a chromosome, the two crossovers nearest to the centromere exhibit four different categories denoted as two chromatids, three chromatids (I), three chromatids (II), and four chromatids (Figure 3H). In our experiment, three out of the four categories can be distinguished and counted, whereas one category, three chromatids (I), cannot be identified because crossovers between the two chromatids are not recognizable in the diploid PB1. The theoretical ratio of the three identifiable categories should be 1:1:1 in the absence of chromatid interference. As shown in Figure 3H, a total count of 440 (35% ± 1%), 440 (35% ± 1%), and 374 (30% ± 1%) was observed for the two chromatids, three chromatids (II), and four chromatids categories, respectively, indicating that there is a weak and negative chromatid interference in human meiosis

Figure 3. Distribution Characteristics of Crossovers in Human Oocytes

(A) Distribution of crossover numbers for single haploid cells (PB2, FPN) and the oocyte triads.

(B) Moderate correlation of crossover numbers in the PB2 and FPN from the same oocyte (R = 0.61).

(C) The personal genetic map of a female individual (donor S01) at 5 Mb resolution, which is largely consistent with that of HapMap and deCODE (female). The recombination rate is denoted with cM/Mb (centimorgans per megabase pair).

(D) Distribution of crossover determination resolution at average sequencing depth of 0.74. Accumulative percentage of crossover numbers is shown as red curve.

(E) Decrease of recombination rate near TSS. cM, centimorgans.

(F) Crossover interference shows a big difference between two sexes on the genomic distance scale.

(G) Crossover interference study with oocyte triad. The distribution of neighboring crossover distances from oocyte triads and the haploid gamete cells (PB2 and FPN) is shown for comparison.

(H) Weak negative chromatid interference within the same chromosome arm. There are four possible recombination categories for chromatid pair selection in a crossover, considering a neighboring crossover on the same chromosome arm. The numbers for each recombination category are counted from the crossover pairs nearest to the centromere in the 55 euploid oocytes. The ratio of the three categories is 35 (± 1%): 35 (± 1%): 30 (± 1%), not 1:1:1, suggesting that there is a negative chromatid interference.

See also Figure S3 and Tables S2, S3, and S4.

(chi-square test, p value 0.03). The positive interference means that having the first crossover between a pair of chromatids decreases the probability of having another crossover between the second pair containing one of the two original chromatids. The negative interference means the reverse. The slight but negative interference is confirmed by our bootstrapping analysis (Figure S3D), which yields the error bars. We note that weak chromatid interference was reported for fungus *N. crassa*, whereas no chromatid interference was reported for yeast (Mancera et al., 2008; Zhao et al., 1995). We are aware of the complications that differences might exist among chromosomes and various genome regions. The weak chromatid interference in human oocytes seen in our experiment calls for further investigations on the underlying mechanism.

In contrast, for crossover pairs on different chromosome arms, only two observable patterns can be identified (Figure S3E). One pattern contains the two chromatids and three chromatids (I) category, whereas the other pattern contains the four chromatids and three chromatids (II) category. We observed an almost equal count, 478 (50%) and 477 (50%), for the two observable patterns, respectively (chi-square test, p value 0.97), the bootstrapping of which was shown in Figure S3F. These results suggest that chromatid interference does not exist when the two crossovers are on the opposite sides of a centromere.

Allele Deduction of a Female Pronucleus by Sequencing the First and Second Polar Bodies

It is highly desirable to determine which sets of alleles are present in an FPN due to homologous recombination without destroying the FPN. In principle, with the knowledge of the donor's haplotypes, the FPN alleles can be easily deduced from those of PB1 and PB2. This deduction is based on the fact that there should be a total of two copies of both paternal and maternal DNA when summing up the PB1, PB2, and FPN from the same oocyte (Figures 4A and 4B). Based on this principle, we can deduce the alleles of an FPN by sequencing its two corresponding polar bodies, which facilitates genome-wide screening of maternal disease-associated alleles in the FPN.

To demonstrate the proof of principle, we sequenced FPNs under the donors' consents and compared it with the deductions from the two corresponding polar bodies. Indeed, 91% of the predicted haplotypes for FPN, 40 out of 44, were confirmed by direct sequencing of the FPNs (Figures 4C and S4). Among the unmatched four oocytes, three have severe DNA degradation in PB1, and one has intrinsic chromosome abnormality (discussed below). When the haplotype of an FPN is determined, all the phased SNPs of the donor are allocated to FPN (Figure 4B). In so doing, the density of predicted alleles for the FPN depends solely on the donor's phased hetSNPs, which can be further improved by other SNP discovering and phasing techniques (Wang et al., 1998), enabling high-accuracy and high-density SNP prediction without destroying the FPN.

Identification of Maternal Mendelian Diseases by MALBAC-Based Genome-wide PGS

About 7,000 monogenic disorders have been estimated (Boycott et al., 2013), which in total occur in about 1 out of every 200 neonates. Usually, every individual carries some heterozygous disease-associated alleles (Abecasis et al., 2012). If this allele is dominant, it is desirable to avoid transmission of this maternal allele to the neonate. If the disease-associated allele is recessive, it is also desirable to avoid transmission of this maternal allele to the neonate in case the father also carries and contributes the disease allele to the baby.

PGD for Mendelian diseases can greatly reduce genetic defects (Sermon et al., 2004). The most widely adopted method for detecting known disease-associated alleles is blastomere biopsy coupled with single-locus PCR (Van de Velde et al., 2000). However, PCR-based PGD can detect only limited numbers of suspected loci due to its low throughput. With the predicted SNPs, we can thoroughly screen undesirable alleles in FPN, which were associated with severe hereditary genetic diseases.

Among the eight donors' heterozygous SNV alleles, we found several potential disease-associated alleles for each donor (Table S5) using the Human Gene Mutation Database (HGMD). Taking donor S08 as an example, we identified three potential disease-associated alleles in genes *AGL*, *GP9*, and *HPD* (Table 1).

Although these diseases are not severe, they provide hypothetical test cases for the ability to call SNVs for embryo selection. In principle, the oocytes containing fewer Mendelian disease-associated alleles can be selected for embryo transfer. We confirmed the predicted alleles by Sanger sequencing of the MALBAC product of the 11 female pronuclei under the donor's consent (Table 1 and Figure S5). For 32 out of 33 loci, Sanger sequencing results were consistent with the predictions, except the one not successfully amplified by MALBAC, and were not able to be analyzed by Sanger sequencing. Overall, this result confirmed the feasibility of detecting and avoiding genome-wide maternal Mendelian disease-associated alleles in fertilized eggs.

Detection of Aneuploidy in Oocytes with High Accuracy and Resolution

Aneuploidy, abnormality of chromosome numbers due to chromosome segregation errors during meiosis, results in miscarriage or genetic disorders of neonates. In PGS, CGH and SNP arrays have been used for aneuploidy screening (Harper and Sengupta, 2012) but with limited resolution. With MALBAC's significantly improved coverage uniformity over other existing whole-genome amplification methods (Zong et al., 2012), the aneuploidy can be confidently determined with the raw coverage depth for an individual oocyte (Figure 5A). Moreover, we found that MALBAC's systematical coverage bias on a finer scale is reproducible genome wide and can be normalized in order to further reduce the bias (Figures S6A and S6B). Using the normalized coverage depth, the copy number can be accurately determined at a megabase resolution (Figure 5A).

In order to measure the signal stability, the SD of normalized coverage depth for each cell was calculated. Most (97%) of the cells showed only slight bias of coverage depth (SD < 0.36) except for six (3%) cells (SD > 0.36), including three PB1, one PB2, and two FPN (Figure 5B). It is difficult to infer the copy number from coverage depth for these six cells, which may be due to DNA degradation, inefficient cell lysis, or MALBAC

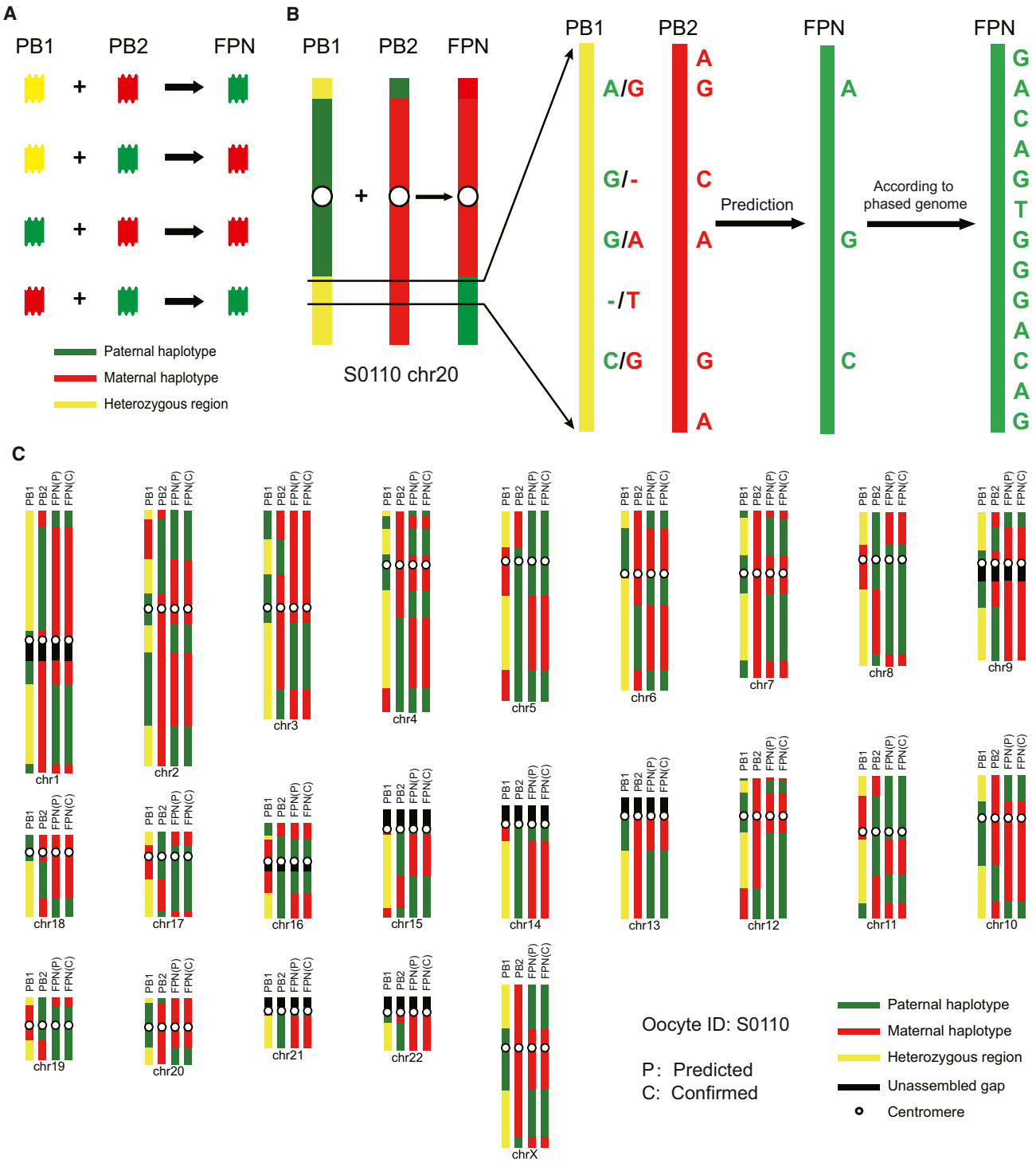

Figure 4. Deduction of the Haplotype of FPN by Sequencing the Genomes of PB1 and PB2

(A) Principle of haplotype deduction for the FPN. For a DNA fragment where no crossover occurs, if PB1 is heterozygous, the haplotype of FPN should be different from that of PB2. Otherwise, the haplotype of FPN should be the same as that of PB2.

(B) Deduction of chromosome haplotype and allocation of genotypes. PB1 and PB2 are separately genotyped, from which the haplotype of FPN is deduced. However, the SNP density of predicted FPN depends on the phased hetSNPs of the donor.

(C) The predicted haplotype of FPN is clearly confirmed by the sequencing results. The haplotypes of PB1, PB2, predicted FPN (left), and sequenced FPN (right) are shown for all the chromosomes from oocyte S0110.

See also Figure S4.

Table 1. Deduction of Mendelian Disease-Associated SNVs in Female Pronuclei of Donor S08

Oocyte ID	Gene Name											
	AGL (C→T)				*GP9* (G→A)				*HPD* (C→T)			
	PB1	PB2	FPN (P)	FPN (C)	PB1	PB2	FPN (P)	FPN (C)	PB1	PB2	FPN (P)	FPN (C)
S0801	N/N	N	T	T	N/N	N	G	G	T/N	C	C	C
S0802	N/N	N	C	C	N/N	N	G	G	N/N	T	T	T
S0803	N/N	N	T	T	N/N	N	G	G	N/N	C	C	C
S0806	N/N	C	C	C	N/N	N	A	A	N/N	N	C	C
S0807	N/N	N	C	C	N/N	N	A	A	N/N	N	C	C
S0808	C/N	T	C	C	N/N	N	A	A	N/N	N	C	C
S0809	C/C	N	T	T	N/N	N	G	G	N/N	T	C	C
S0811	N/N	T	T	T	N/N	N	A	A	N/N	N	C	C
S0812	C/C	T	T	T	N/N	N	G	Δ	C/T	N	T	T
S0813	N/N	C	T	T	N/N	N	G	G	N/N	T	C	C
S0815	N/N	N	C	C	N/N	N	A	A	N/N	N	T	T

For this donor, the corresponding genotypes for 11 FPNs of the oocytes, which have all the PB1, PB2, and FPN recovered and sequenced, are predicted by the haplotype deduction. The "N" represents the alleles that are not covered by single-cell low-depth sequencing. The underlined bases represent SNVs associated with Mendelian diseases. Δ represents the allele that could not be amplified by locus-specific PCR from single-cell MALBAC product. Although some SNP loci are not covered by low-depth sequencing in polar bodies, the genotype of FPN can still be accurately predicted by the haplotype information. See also Figure S5 and Table S5.

amplification bias. Luckily, the predetermined haplotype information of the cell, which is less sensitive to coverage depth bias, can be used to determine the chromosome copy number for five of the six cells successfully.

Besides chromosomal-level aneuploidy, the detection of missing (or duplication of) smaller DNA segments is also important, so we tried to figure out the resolution limit of this method. We observed that the normalized coverage depth curve is quite uniform (SD < 0.15) at larger than megabase resolution but gets very noisy (SD > 2.5) at resolution down to 10 kb (Figures 5C and S6C). Then we estimated the sensitivity and specificity of aneuploidy detection under different resolutions using the resolved ploidy information of our oocytes as a reference. We found that both sensitivity and specificity get higher for lower resolutions, and it achieves 97.8% sensitivity and 99.5% specificity at 5 Mb resolution (Figure 5C). In fact, for submegabase resolution (0.5 Mb), it achieves 94.8% sensitivity and 97.5% specificity, which is superior to most available CGH and SNP array technologies (Coe et al., 2007).

Aneuploidy in Oocytes

A primary oocyte replicates its diploid genome at prophase I, forming four copies of chromatids (4C) that are segregated in sequential two meiotic divisions to generate PB1, PB2, and FPN. To assess the possibility that aneuploidy arose from the DNA replication, we checked the sum of the chromatids in PB1, PB2, and FPN from each oocyte and found that the majority (43 out of 44) of the primary oocytes implement DNA replication with high fidelity. Surprisingly, the oocyte S0608 showed a loss of four chromatids in FPN and a loss of one chromatid in PB2, whereas no gain of chromatids was detected in PB1 (Figure S6D), which may be caused by the failure of DNA replication or more likely the wrong segregation of chromosomes during cell division, such as aberrant segregation of a chromosome from the whole chromosome set due to an abnormal break of the spindle (Vogt et al., 2008).

Compared to DNA replication, chromosome segregation in oocytes is more error prone, probably due to loss of cohesions, DSBs, or other lesions during long time span of female meiosis (Kurahashi et al., 2012). We detected 12 aneuploid oocytes from 8 donors due to abnormal chromatid segregation (Table S6). The aneuploid chromosomes showed clear patterns of missing or gaining coverage depth, whereas the other chromosomes showed normal coverage depth (Figure S6E). The average aneuploidy rate for all of the donors is 17.6%, which is reasonable considering the relatively young ages of the donors (Figure 5D) (Munné et al., 2007). In the 12 aneuploid oocytes, we detected 28 aneuploid chromosomes, among which meiosis I error rate is much higher than that of meiosis II, and numerical (whole chromosome) abnormalities are more common than structural (part of chromosome) abnormalities (Hassold et al., 2007) (Figure 5E). Chromosomes 16 and 22 are the most common aneuploid chromosomes, which is consistent with previous reports (Pellestor et al., 2002).

Lower Crossover Activity in Aneuploid Oocytes

Homologous recombination is pertinent for proper chromosome segregation in meiosis (Page and Hawley, 2003), and the reduction in crossover activity of the whole gamete has been reported in abnormal sperm (Hann et al., 2011; Lu et al., 2012). Our method is able to detect crossover and aneuploidy simultaneously, giving us the chance to study the relationship between them. We found that 26 of 28 aneuploid chromosomes do have crossovers on their sister chromatids, confirming the theory that each pair of homologous chromosomes has at least one crossover (Mets and Meyer, 2009). The reduction of crossover activity has been reported for many trisomies (Hassold et al., 1995), and our data also show significant reduction of crossover activity for

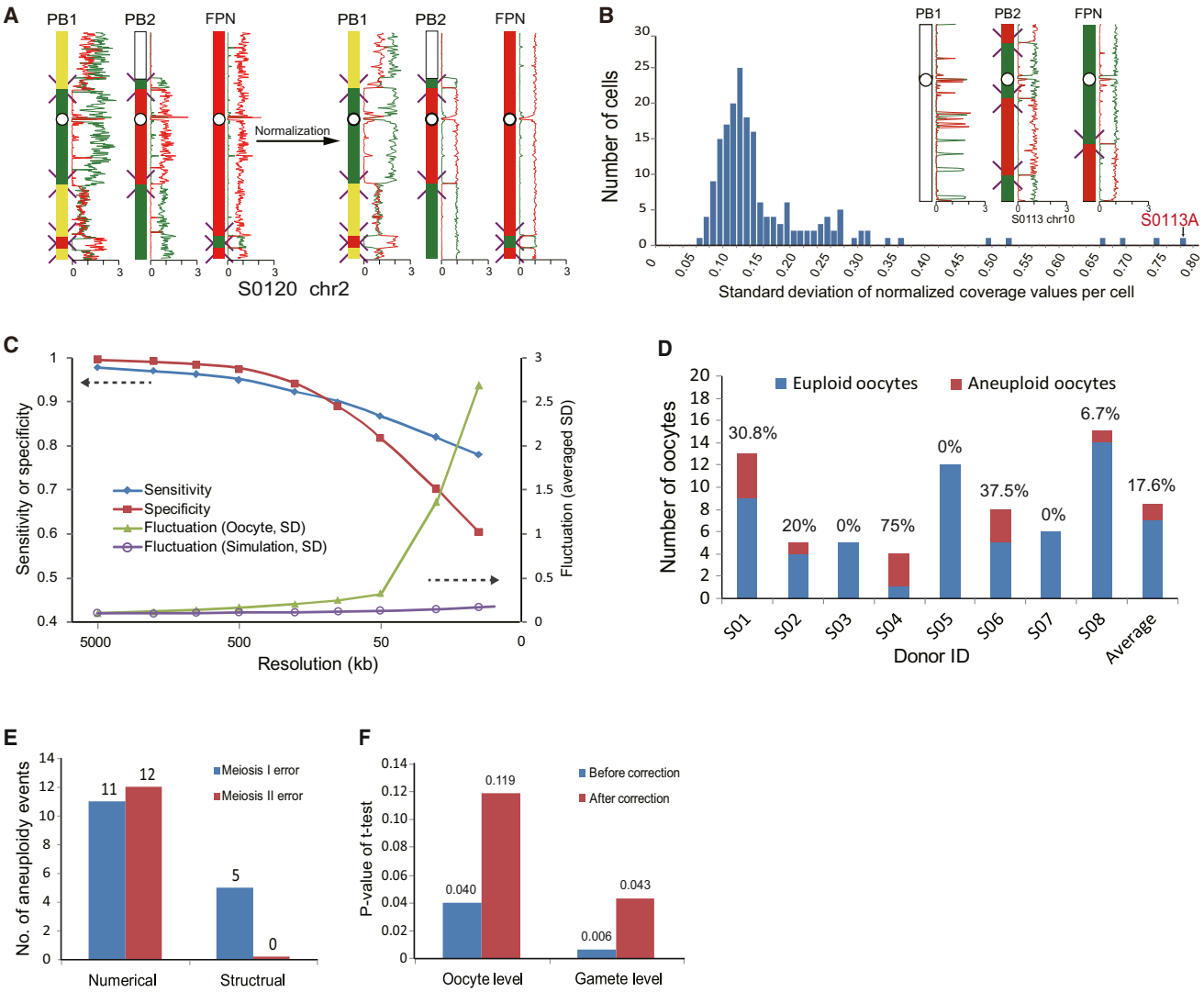

Figure 5. High-Resolution and Accurate Detection of Aneuploidies Facilitates the Study of Aneuploidy Characteristics

(A) Coverage depth after normalization is used to infer the copy number of chromosome segments. A terminal segment of the short arm of chromosome 2 is missing in PB2, whereas PB1 has an additional copy of it.

(B) Fluctuation of normalized coverage depth denoted by SD is low for most of the sequenced single cells, except for six cells (SD > 0.36). S0113A is the cell with the most severe fluctuation. As an example, chromosome 10 of this cell and its corresponding PB2 and FPN are shown on the top-right corner.

(C) Sensitivity and specificity of aneuploidy detection under various resolutions. The resolved ploidy information of the oocytes was used as a reference. Note that the six cells with severe coverage fluctuation and four cells with severe contamination are not used for statistical analysis here. If the expected copy number is n, then the normalized coverage depth values falling in range of n ± 0.5 were taken as a correct prediction. The averaged SD values under various resolutions are also shown in comparison with values from simulated sequencing data without any coverage bias.

(D) Comparison of aneuploidy rate among the donors.

(E) Attribution of numerical and structural abnormality to specific meiosis stage.

(F) Difference of crossover numbers between aneuploid and euploid oocyte triads and gamete cells illustrated by p values of Student's t test. To correct the inefficiency of crossover detection in aneuploid chromosomes, we replaced the crossover numbers in the aneuploid chromosomes by randomly choosing one from the corresponding euploid oocytes. The process was repeated 100 times, and the p values were averaged. After correction, the significance level goes down (p value gets higher) for both the oocyte triad and gamete cell levels.

See also Figure S6 and Table S6.

aneuploid chromosomes using the same statistics method (p value 3×10^{-4}) (Figure S6F). However, these may not be all of the facts. As the crossovers between the two nondisjunction chromatids that went into the same aneuploid gamete are hard to detect from current data, the crossover rate for aneuploid chromosomes is likely to be underestimated, which contributes partially to the observed reduction in crossover activity.

We compared the crossover numbers from the aneuploidy and euploidy groups on both the single-haploid-cell level and oocyte triad level and observed significantly lower crossover

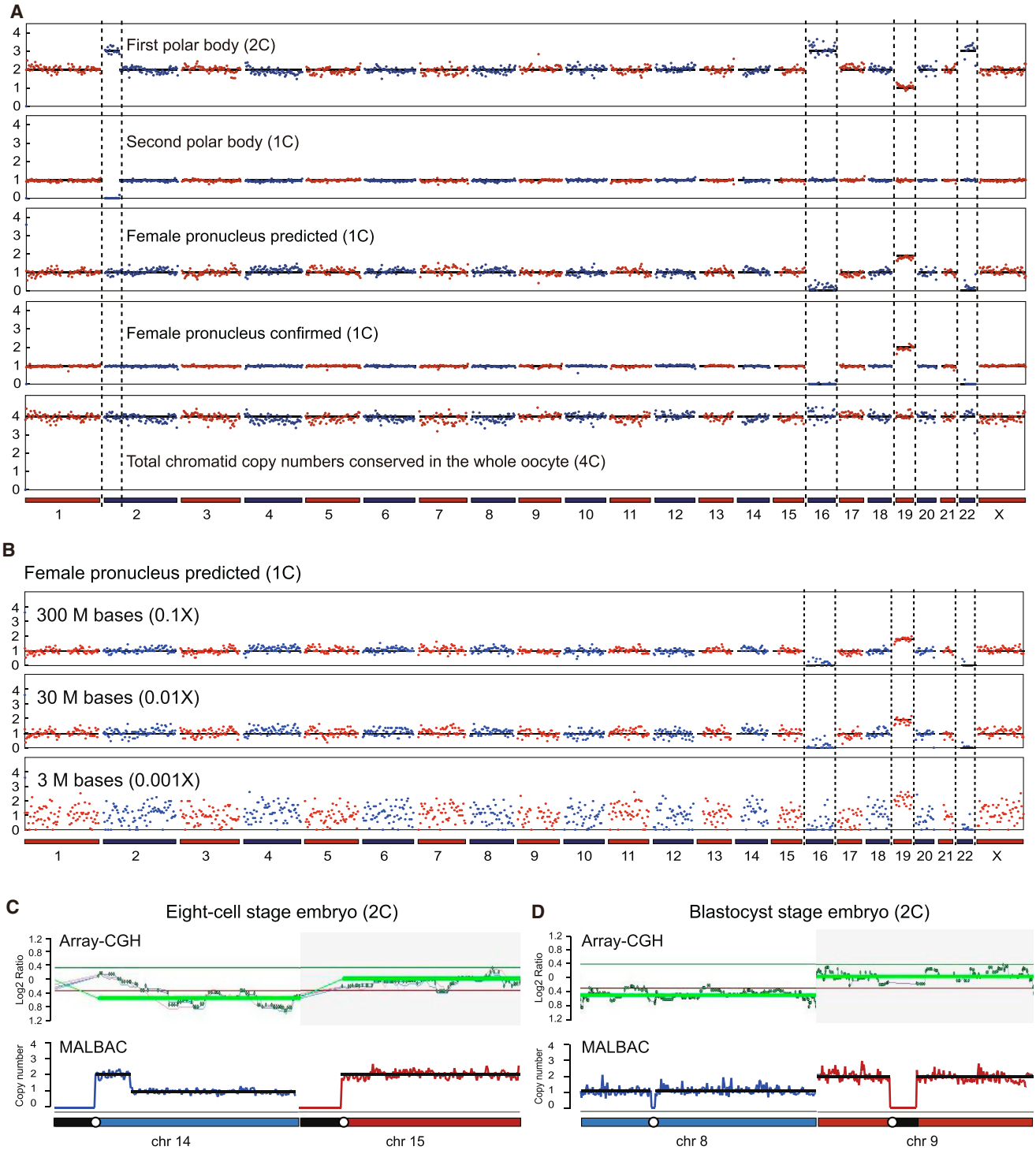

Figure 6. Deduction of Aneuploidy in IVF

(A) Copy number of chromosomes of FPN can be deduced by its two polar bodies. On the basis of constant total copy number of each genome locus of oocyte cells (PB1, PB2, FPN), we predict the copy number (black lines) and normalized coverage depth (red or blue dots) for the FPN in 3 Mb windows along the genome by subtracting the corresponding values of PB1 and PB2 from 4. As an example, the FPN of oocyte S0120 is predicted to have an additional chromosome 19 but miss chromosome 16 and 22, which was further confirmed by the FPN sequencing.

(B) Influence of sequencing depth on aneuploidy deduction. Three levels of sequencing depth (0.1×, 0.01×, and 0.001×) were analyzed, and the results suggest that 0.01× data are sufficient for aneuploidy deduction at megabase resolutions.

(legend continued on next page)

activity for the aneuploidy group (t test, p = 0.006, on cell level; p = 0.04, on oocyte triad level) (Figure 5F). The smaller difference for the oocyte level (higher p value) may be caused by the larger average number of crossovers and thus less sensitivity to variations.

To account for the crossover detection defects in aneuploid chromosomes, we replaced the crossover count on aneuploid chromosomes by randomly choosing a counterpart from the euploid group. The p values on both the single-haploid cell and oocyte level became higher (0.043 and 0.119, averaged by 100 times bootstrapping). An alternative way to make up the detection defects is to exclude the crossover count of aneuploid chromosomes from both the aneuploidy and euploidy groups for statistical analysis (Figure S6G). The results of both analyses supported that the crossover activity for the aneuploid oocyte is a little lower than that of the euploid oocyte, but not so much as the previous studies reported (Bugge et al., 1998; Hassold et al., 1991).

Deducing Aneuploidy of an Oocyte Based on Polar Body Sequencing in PGS

As discussed above, aneuploidy of the FPN can be deduced with the ploidy of the first and second polar bodies without destroying the fertilized egg. Figure 6A shows the normalized read density across the 23 chromosomes of the PB1 of the oocyte S0120, in which aneuploidy is clearly seen at chromosomes 2, 16, 19, and 22. It also shows the data for the corresponding PB2 of the same oocyte, which has a partial aneuploidy at chromosome 2. We then predicted what is in the FPN by subtracting the PB1 and PB2 from 4, which is the expected total number of chromatids.

To verify the prediction, we directly sequenced the female pronucleus in the same oocyte under the consent of the donor. Indeed, the prediction is experimentally verified. As a final check, we added up the data from PB1, PB2, and the female pronucleus; the number 4 is conserved along the entire genome (Figure 6A). This result demonstrated the proof of principle of the IVF procedure for selecting a viable fertilized egg for transfer.

To estimate the minimum sequencing depth needed to accurately detect aneuploidy in an oocyte cell, we carried out data analyses by taking a subset of the data from the three cells of oocyte S0120. The results of predicted copy number for the FPN with data amount of 3 M (million bases) (0.001×), 30 M (0.01×), and 300 M (0.1×) are shown in Figure 6B, and the results of PB1, PB2, and confirmed FPN are shown in Figure S7A. It is evident that sequencing data as little as 30 M (0.01×) can confidently detect aneuploidy.

At submegabase resolution (0.5 Mb), there is no significant decrease in detection sensitivity when reducing the sequencing depth from 1× to 0.01× (Figures S7B and S7C). As aneuploidy often spans an entire chromosome, this submegabase resolution is sufficient to determine aneuploidy. The fact that a sequencing depth of only 0.01× is needed is highly desirable in order to decrease the cost of PGS in IVF (Table S7).

Comparison with Array CGH

We compared our MALBAC sequencing method with the array CGH method in accuracy for detecting aneuploidies. An eight-cell-stage embryo was donated by a couple who already had one healthy baby from the same oocyte retrieval cycle and donated their remaining frozen embryos for scientific research and signed informed consent. We isolated two individual cells from the eight-cell-stage embryo and analyzed one cell with MALBAC whole-genome sequencing analysis while examining the other cell with array CGH analysis with MDA amplification. As shown in Figure 6C, at whole-genome scale, both methods can accurately detect aneuploidies. Furthermore, with as low as 0.1× sequencing depth, MALBAC sequencing results show digitized signals with much less fluctuation and higher resolution (0.5 Mb) than the array CGH result (about 2.5 Mb).

Sequencing Blastocysts with MALBAC

When disease-associated SNVs or aneuploidy might come from the father, PGD/PGS have been carried out with array CGH for blastocyst biopsy (Broman et al., 1998). A blastocyst-stage embryo was donated by a couple with the male partner known to be a carrier of a specific genetic disease. After detection of the mutation and aneuploidy of these blastocysts by MALBAC sequencing, one of the aneuploid embryos was also analyzed by array CGH under the consent of the patient. That is, two small clumps of a few trophectoderm cells were isolated from the blastocyst-stage embryo and were analyzed by MALBAC and array CGH methods side by side, as shown in Figure 6D. Clearly, the MALBAC result is less noisy and of higher resolution.

DISCUSSION

We have successfully applied whole-genome amplification based on MALBAC to single human oocytes, extending the analyses of single human sperm cells (Lu et al., 2012; Wang et al., 2012). The genome coverage for a single oocyte cell when sequenced at 1× is ~32%, which is higher than that reported for a single sperm cell (~20%) with comparable sequencing depth (Lu et al., 2012) probably because of the looser chromatin structure of oocytes. Distinctly different from sperm, the oocytes exhibit several features in meiosis, such as higher recombination rates and higher aneuploidy rates, yielding the first comprehensive analyses of female meiosis recombination.

(C) Comparison of aneuploidy deduction between MALBAC sequencing and array CGH method for an eight-cell-stage embryo. Two individual cells from an aneuploid eight-cell-stage embryo were analyzed by these two independent methods. Chromosome 14 shows loss of a large segment of its long arm. The resolution is 0.5 Mb for MALBAC sequencing, whereas the resolution is 2.5 Mb for array CGH.

(D) Comparison of aneuploidy deduction between MALBAC sequencing and array CGH method for a blastocyst stage embryo. Two small clumps of a few trophectoderm cells were isolated from an aneuploid blastocyst-stage embryo and analyzed by these two independent methods. There is a whole-chromosome aneuploidy for chromosome 8. The resolution is 0.5 Mb for MALBAC sequencing, whereas the resolution is about 2.5 Mb for array CGH.

See also Figure S7 and Table S7.

This study not only provides information about meiosis of human oocytes but also yields a procedure for PGS in IVF. Although more blastocyst biopsies have currently been used in PGD/PGS, the polar body biopsy has advantages when aneuploidies and disease alleles are inherited from the mother. First, the polar body biopsy is performed on the oocyte retrieval day (day 0) rather than day 5, so more time is available for sequencing and analyses, especially if freezing of embryos needs to be avoided. Second, blastocyst biopsy removes cells from the growing embryo, whereas the polar body biopsy removes genetic material that is dispensable for embryonic development. However the disadvantages for polar body biopsy are that it cannot detect the aneuploidies and mutations inherited from the father and cannot detect the aneuploidies and de novo mutations arising from mitosis.

By sequencing the first and second polar bodies, we have provided proof of principle for a low-cost PGS procedure of selecting fertilized eggs for transfer that are free of maternal aneuploidy and alleles associated with Mendelian diseases. The same method in principle can be applied to blastocysts, considering that the severe genetic variation is either from the father or the mother. Our MALBAC sequencing offers improved resolution and accuracy of simultaneous detection of chromosome abnormality and heterozygous SNVs associated with Mendelian diseases. The aneuploidy detection by next-generation sequencing is comparable or even less expensive than CGH arrays, whereas the disease SNV calling is still costly. As the sequencing costs decrease rapidly, by offering more accurate information, our single-cell amplification method will gain more advantages in the future. Such a single-cell manipulation and diagnosis allows probing and bettering of life at the single-molecule level.

EXPERIMENTAL PROCEDURES

Donor Recruitment and Oocyte Retrieval

This study has been approved by the Reproductive Study Ethics Committee at Peking University Third Hospital (research license 2012SZ014). All oocytes and sperm were obtained with informed consent, which confirmed that donors voluntarily donated oocytes and sperm. All of the procedures for oocyte collection and operation were performed following standard clinical protocols (Li et al., 2008). The oocyte donors have already had one or two healthy children from natural pregnancy, and they donated their oocytes purely for research purposes.

Isolation and MALBAC Whole-Genome Amplification of Single Polar Bodies and Pronuclei

The first polar bodies (PB1) and second polar bodies (PB2) were sequentially picked after ICSI. The male and female pronuclei were removed after the zygote entered pronuclear stage. Each single-cell sample was assigned a unique cell ID beginning with an "S," followed by a four-digit number and an alphabetic letter. Suffixes of single-cell ID "A, B, and C" mean PB1, PB2, and FPN, respectively. Each polar body or pronucleus was transferred into individual PCR tubes and lysed in 5 μl lysis buffer. The DNA released from the lysed cell in each tube was amplified using MALBAC (Zong et al., 2012).

High-Throughput Sequencing and Prefiltering of the Sequencing Data

The qualified amplified genomic DNA was used to construct Illumina libraries for high-throughput sequencing. The MALBAC amplification primers, Illumina library adapters, and unreliable low-quality read ends were trimmed from the raw sequencing data.

Calling of Heterozygous SNPs for the Donor and Genotype Determination of the Oocyte Cells

The confident heterozygous SNPs for each donor were determined by integrating all the genotype likelihoods of all her oocyte cells. With the donor's heterozygous SNP information, the posterior probabilities for each SNP allele were estimated in each oocyte cell by the Bayesian theory.

Phasing Heterozygous SNPs and Inferring Genome Positions of Crossovers

The hetSNPs of the donor were phased, and the genome positions of crossovers were inferred in all oocyte cells by two independent algorithms, and these two algorithms generated largely consistent results. Additional details are provided in the Extended Experimental Procedures.

Normalization of Coverage Depth and Aneuploidy Detection

For each cell, the normalized coverage depth was calculated by dividing the averaged raw depth of several cells from the same window, as well as the sequencing depth of the given sample. Aneuploidy was identified when the observed copy number was different from the expected ones.

ACCESSION NUMBERS

The sequencing data have been deposited in the National Center for Biotechnology Information under the accession number SRA091188.

SUPPLEMENTAL INFORMATION

Supplemental Information includes Extended Experimental Procedures, seven figures, and seven tables and can be found with this article online at http://dx.doi.org/10.1016/j.cell.2013.11.040.

AUTHOR CONTRIBUTIONS

Y.H. and L.X. performed experiments, including single-cell genome amplification, by using MALBAC technique, preparing sequencing libraries, and verifying candidate SNVs. W.F. and J.L. worked on the bioinformatic analysis, including writing the computer codes, building personal crossover maps, systematic data mining, and all of the statistical analysis. L.Y. and R.L. worked on recruiting voluntary donors, performing IVF procedures, and collecting zygotes. Y.L. and J.H. isolated polar bodies and male and female pronuclei by micromanipulation. J.Q., F.T., and S.X. conceived the experiment, supervised the project, and wrote the manuscript with help from all of the authors.

ACKNOWLEDGMENTS

J.Q. and F.T. were supported by grants from the National Basic Research Program of China (2011CB944500, 2012CB966704, and 2011CB966303) and grants from the National Natural Science of China (31230047, 31322037, and 31271543). X.S.X., F.T., and J.Q. were supported by a grant from the Beijing Municipal Science and Technology Commission (Z131100005213006) and a Peking University grant for translational research. L.Y. was supported by a grant from the National Natural Science Foundation of China (81000275). The authors would like to acknowledge the oocyte and sperm donor volunteers and the staff at the Peking University Third Hospital for recruiting donors and collecting samples. We acknowledge the staff of the BIOPIC sequencing facility at Peking University for assistance. We also thank A.R. Chapman, J. Zhang, C. Zong, S. Lu, and A. Surani for helpful discussions. We sincerely thank N. Kleckner for providing us with helpful advice on the manuscript.

Received: September 27, 2013
Revised: October 31, 2013
Accepted: November 25, 2013
Published: December 19, 2013

REFERENCES

Abecasis, G.R., Auton, A., Brooks, L.D., DePristo, M.A., Durbin, R.M., Handsaker, R.E., Kang, H.M., Marth, G.T., and McVean, G.A.; 1000 Genomes Project Consortium (2012). An integrated map of genetic variation from 1,092 human genomes. Nature *491*, 56–65.

Bansal, V., Harismendy, O., Tewhey, R., Murray, S.S., Schork, N.J., Topol, E.J., and Frazer, K.A. (2010). Accurate detection and genotyping of SNPs utilizing population sequencing data. Genome Res. *20*, 537–545.

Boycott, K.M., Vanstone, M.R., Bulman, D.E., and MacKenzie, A.E. (2013). Rare-disease genetics in the era of next-generation sequencing: discovery to translation. Nat. Rev. Genet. *14*, 681–691.

Broman, K.W., Murray, J.C., Sheffield, V.C., White, R.L., and Weber, J.L. (1998). Comprehensive human genetic maps: individual and sex-specific variation in recombination. Am. J. Hum. Genet. *63*, 861–869.

Bugge, M., Collins, A., Petersen, M.B., Fisher, J., Brandt, C., Hertz, J.M., Tranebjaerg, L., de Lozier-Blanchet, C., Nicolaides, P., Brøndum-Nielsen, K., et al. (1998). Non-disjunction of chromosome 18. Hum. Mol. Genet. *7*, 661–669.

Chen, S.Y., Tsubouchi, T., Rockmill, B., Sandler, J.S., Richards, D.R., Vader, G., Hochwagen, A., Roeder, G.S., and Fung, J.C. (2008). Global analysis of the meiotic crossover landscape. Dev. Cell *15*, 401–415.

Cheng, E.Y., Hunt, P.A., Naluai-Cecchini, T.A., Fligner, C.L., Fujimoto, V.Y., Pasternack, T.L., Schwartz, J.M., Steinauer, J.E., Woodruff, T.J., Cherry, S.M., et al. (2009). Meiotic recombination in human oocytes. PLoS Genet. *5*, e1000661.

Coe, B.P., Ylstra, B., Carvalho, B., Meijer, G.A., Macaulay, C., and Lam, W.L. (2007). Resolving the resolution of array CGH. Genomics *89*, 647–653.

Coop, G., Wen, X., Ober, C., Pritchard, J.K., and Przeworski, M. (2008). High-resolution mapping of crossovers reveals extensive variation in fine-scale recombination patterns among humans. Science *319*, 1395–1398.

Drouaud, J., Mercier, R., Chelysheva, L., Bérard, A., Falque, M., Martin, O., Zanni, V., Brunel, D., and Mézard, C. (2007). Sex-specific crossover distributions and variations in interference level along Arabidopsis thaliana chromosome 4. PLoS Genet. *3*, e106.

Ferguson, K.A., Wong, E.C., Chow, V., Nigro, M., and Ma, S. (2007). Abnormal meiotic recombination in infertile men and its association with sperm aneuploidy. Hum. Mol. Genet. *16*, 2870–2879.

Fonseka, K.G., and Griffin, D.K. (2011). Is there a paternal age effect for aneuploidy? Cytogenet. Genome Res. *133*, 280–291.

Fung, J.C., Rockmill, B., Odell, M., and Roeder, G.S. (2004). Imposition of crossover interference through the nonrandom distribution of synapsis initiation complexes. Cell *116*, 795–802.

Hann, M.C., Lau, P.E., and Tempest, H.G. (2011). Meiotic recombination and male infertility: from basic science to clinical reality? Asian J. Androl. *13*, 212–218.

Harper, J.C., and Sengupta, S.B. (2012). Preimplantation genetic diagnosis: state of the art 2011. Hum. Genet. *131*, 175–186.

Hassold, T.J., Sherman, S.L., Pettay, D., Page, D.C., and Jacobs, P.A. (1991). XY chromosome nondisjunction in man is associated with diminished recombination in the pseudoautosomal region. Am. J. Hum. Genet. *49*, 253–260.

Hassold, T., Merrill, M., Adkins, K., Freeman, S., and Sherman, S. (1995). Recombination and maternal age-dependent nondisjunction: molecular studies of trisomy 16. Am. J. Hum. Genet. *57*, 867–874.

Hassold, T., Hall, H., and Hunt, P. (2007). The origin of human aneuploidy: where we have been, where we are going. Hum. Mol. Genet. *16*, R203–R208.

Hunt, P.A., and Hassold, T.J. (2002). Sex matters in meiosis. Science *296*, 2181–2183.

Jeffreys, A.J., Murray, J., and Neumann, R. (1998). High-resolution mapping of crossovers in human sperm defines a minisatellite-associated recombination hotspot. Mol. Cell *2*, 267–273.

Kirkness, E.F., Grindberg, R.V., Yee-Greenbaum, J., Marshall, C.R., Scherer, S.W., Lasken, R.S., and Venter, J.C. (2013). Sequencing of isolated sperm cells for direct haplotyping of a human genome. Genome Res. *23*, 826–832.

Kleckner, N. (2006). Chiasma formation: chromatin/axis interplay and the role(s) of the synaptonemal complex. Chromosoma *115*, 175–194.

Kleckner, N., Storlazzi, A., and Zickler, D. (2003). Coordinate variation in meiotic pachytene SC length and total crossover/chiasma frequency under conditions of constant DNA length. Trends Genet. *19*, 623–628.

Kong, A., Thorleifsson, G., Gudbjartsson, D.F., Masson, G., Sigurdsson, A., Jonasdottir, A., Walters, G.B., Jonasdottir, A., Gylfason, A., Kristinsson, K.T., et al. (2010). Fine-scale recombination rate differences between sexes, populations and individuals. Nature *467*, 1099–1103.

Kurahashi, H., Tsutsumi, M., Nishiyama, S., Kogo, H., Inagaki, H., and Ohye, T. (2012). Molecular basis of maternal age-related increase in oocyte aneuploidy. Congenit. Anom. (Kyoto) *52*, 8–15.

Li, R., Qiao, J., Wang, L., Zhen, X., and Lu, Y. (2008). Serum progesterone concentration on day of HCG administration and IVF outcome. Reprod. Biomed. Online *16*, 627–631.

Liss, J., Mirecka, A., Kitowska, K., and Lukaszuk, K. (2011). Preimplantaion genetic diagnosis of hearing loss with 35delG mutation in GJB2 gene - preliminary report. Otolaryngol. Pol. *65*, 443–446.

Lu, S., Zong, C., Fan, W., Yang, M., Li, J., Chapman, A.R., Zhu, P., Hu, X., Xu, L., Yan, L., et al. (2012). Probing meiotic recombination and aneuploidy of single sperm cells by whole-genome sequencing. Science *338*, 1627–1630.

Mancera, E., Bourgon, R., Brozzi, A., Huber, W., and Steinmetz, L.M. (2008). High-resolution mapping of meiotic crossovers and non-crossovers in yeast. Nature *454*, 479–485.

Mets, D.G., and Meyer, B.J. (2009). Condensins regulate meiotic DNA break distribution, thus crossover frequency, by controlling chromosome structure. Cell *139*, 73–86.

Munné, S., Chen, S., Colls, P., Garrisi, J., Zheng, X., Cekleniak, N., Lenzi, M., Hughes, P., Fischer, J., Garrisi, M., et al. (2007). Maternal age, morphology, development and chromosome abnormalities in over 6000 cleavage-stage embryos. Reprod. Biomed. Online *14*, 628–634.

Myers, S., Bottolo, L., Freeman, C., McVean, G., and Donnelly, P. (2005). A fine-scale map of recombination rates and hotspots across the human genome. Science *310*, 321–324.

Myers, S., Freeman, C., Auton, A., Donnelly, P., and McVean, G. (2008). A common sequence motif associated with recombination hot spots and genome instability in humans. Nat. Genet. *40*, 1124–1129.

Novak, I., Wang, H., Revenkova, E., Jessberger, R., Scherthan, H., and Höög, C. (2008). Cohesin Smc1beta determines meiotic chromatin axis loop organization. J. Cell Biol. *180*, 83–90.

Page, S.L., and Hawley, R.S. (2003). Chromosome choreography: the meiotic ballet. Science *301*, 785–789.

Panizza, S., Mendoza, M.A., Berlinger, M., Huang, L., Nicolas, A., Shirahige, K., and Klein, F. (2011). Spo11-accessory proteins link double-strand break sites to the chromosome axis in early meiotic recombination. Cell *146*, 372–383.

Pellestor, F., Andréo, B., Arnal, F., Humeau, C., and Demaille, J. (2002). Mechanisms of non-disjunction in human female meiosis: the co-existence of two modes of malsegregation evidenced by the karyotyping of 1397 in-vitro unfertilized oocytes. Hum. Reprod. *17*, 2134–2145.

Petkov, P.M., Broman, K.W., Szatkiewicz, J.P., and Paigen, K. (2007). Crossover interference underlies sex differences in recombination rates. Trends Genet. *23*, 539–542.

Qiao, J., Wang, Z.B., Feng, H.L., Miao, Y.L., Wang, Q., Yu, Y., Wei, Y.C., Yan, J., Wang, W.H., Shen, W., et al. (2013). The root of reduced fertility in aged women and possible therapentic options: Current status and future perspects. Mol. Aspects Med. Published online June 21, 2013. http://dx.doi.org/10.1016/j.mam.2013.06.001.

Sermon, K., Van Steirteghem, A., and Liebaers, I. (2004). Preimplantation genetic diagnosis. Lancet *363*, 1633–1641.

Speed, T.P., McPeek, M.S., and Evans, S.N. (1992). Robustness of the no-interference model for ordering genetic markers. Proc. Natl. Acad. Sci. USA *89*, 3103–3106.

Tease, C., and Hultén, M.A. (2004). Inter-sex variation in synaptonemal complex lengths largely determine the different recombination rates in male and female germ cells. Cytogenet. Genome Res. *107*, 208–215.

Teuscher, F., Brockmann, G.A., Rudolph, P.E., Swalve, H.H., and Guiard, V. (2000). Models for chromatid interference with applications to recombination data. Genetics *156*, 1449–1460.

Treff, N.R., Fedick, A., Tao, X., Devkota, B., Taylor, D., and Scott, R.T., Jr. (2013). Evaluation of targeted next-generation sequencing-based preimplantation genetic diagnosis of monogenic disease. Fertil. Steril. *99*, 1377–1384.

Van de Velde, H., De Vos, A., Sermon, K., Staessen, C., De Rycke, M., Van Assche, E., Lissens, W., Vandervorst, M., Van Ranst, H., Liebaers, I., and Van Steirteghem, A. (2000). Embryo implantation after biopsy of one or two cells from cleavage-stage embryos with a view to preimplantation genetic diagnosis. Prenat. Diagn. *20*, 1030–1037.

Van den Veyver, I.B., Patel, A., Shaw, C.A., Pursley, A.N., Kang, S.H., Simovich, M.J., Ward, P.A., Darilek, S., Johnson, A., Neill, S.E., et al. (2009). Clinical use of array comparative genomic hybridization (aCGH) for prenatal diagnosis in 300 cases. Prenat. Diagn. *29*, 29–39.

Vogt, E., Kirsch-Volders, M., Parry, J., and Eichenlaub-Ritter, U. (2008). Spindle formation, chromosome segregation and the spindle checkpoint in mammalian oocytes and susceptibility to meiotic error. Mutat. Res. *651*, 14–29.

Wang, D.G., Fan, J.B., Siao, C.J., Berno, A., Young, P., Sapolsky, R., Ghandour, G., Perkins, N., Winchester, E., Spencer, J., et al. (1998). Large-scale identification, mapping, and genotyping of single-nucleotide polymorphisms in the human genome. Science *280*, 1077–1082.

Wang, J., Fan, H.C., Behr, B., and Quake, S.R. (2012). Genome-wide single-cell analysis of recombination activity and de novo mutation rates in human sperm. Cell *150*, 402–412.

Zhao, H., McPeek, M.S., and Speed, T.P. (1995). Statistical analysis of chromatid interference. Genetics *139*, 1057–1065.

Zong, C., Lu, S., Chapman, A.R., and Xie, X.S. (2012). Genome-wide detection of single-nucleotide and copy-number variations of a single human cell. Science *338*, 1622–1626.